



Rapid retreat of permafrost coastline observed with aerial drone photogrammetry

Andrew M. Cunliffe^{1,2}, George Tanski^{3,4}, Boris Radosavljevic⁵, William F. Palmer⁶, Torsten Sachs⁵, Hugues Lantuit⁴, Jeffrey T. Kerby⁷, and Isla H. Myers-Smith²

5 ‡ These authors contributed equally to this work.

¹ Geography, University of Exeter, Exeter, EX4 4RJ, UK

² School of GeoScience, University of Edinburgh, Edinburgh, UK

³ Faculty of Sciences, Earth and Climate, Vrije Universiteit Amsterdam, Amsterdam, The Netherlands

10 ⁴ Department of Permafrost Research, Alfred Wegener Institute, Helmholtz Centre for Polar and Marine Research, Potsdam, Germany

⁵ GFZ German Research Centre for Geosciences, Helmholtz-Centre, Potsdam, Germany

⁶ Landscapes, Paris, France

⁷ Neukom Institute for Computational Science, Dartmouth College, NH, USA

15 *Correspondence to:* Andrew M. Cunliffe (a.cunliffe@exeter.ac.uk)

Abstract.

Permafrost landscapes are changing around the Arctic in response to climate warming, with coastal erosion being one of the most prominent and hazardous features. Using drone platforms, satellite images and historic aerial photos, we observed the rapid retreat of a permafrost coastline on Qikiqtaruk – Herschel Island, Yukon Territory, in the Canadian Beaufort Sea. Erosion of this coast increasingly threatens the settlement located on the Kuvluraq – Simpson Point gravel spit. This spit accommodates several culturally significant sites and is the logistical base for the Qikiqtaruk – Herschel Island Territorial Park operations. The objectives of this study were to demonstrate the effective use of low-cost lightweight drones for: (i) assessing short-term coastal erosion dynamics over fine temporal resolution, (ii) evaluating short-term change detection in the context of long-term observations of shoreline change, and (iii) demonstrating the potential of these measurement tools for park management and decision makers. Using drones, we resurveyed a 500 m permafrost coastal reach at high temporal frequency (seven surveys over 40 days in 2017). The observed intra-seasonal shoreline changes were related to meteorological and oceanographic variables to understand intra-seasonal erosion dynamics. To put our short-term observations into historical context, we integrated analysis of shoreline positions in 2016 and 2017 with historical observations from 1952, 1970, 2000, and 2011. We found drone surveys analysed with image-based modelling yield fine-grain and accurately geolocated observations that are highly suitable to observe intra-seasonal erosion dynamics. In 2017, we observed coastal retreat of 14.5 m a^{-1} , more than six times faster than the long-term average rate of $2.2 \pm 0.2 \text{ m a}^{-1}$ (1952-2017). Over a single 4 day period, coastline retreat exceeded $1 \pm 0.1 \text{ m d}^{-1}$. Our findings highlight the episodic nature of shoreline change, which is poorly understood along permafrost coastlines. We conclude that the data available from drones is an effective tool to understand better the mechanistic



short-term controls on coastal erosion dynamics and thus long-term coastline change, and has strong potential to support local management decisions regarding coastal settlements in rapidly changing Arctic landscapes.

1 Introduction

The Arctic is the most rapidly warming region on Earth (Richter-Menge et al., 2017; Serreze and Barry, 2011). Increasing
5 temperatures result in fundamental changes to the physical and biological processes that shape these permafrost landscapes
(IPCC, 2013). Permafrost in the Northern Hemisphere is substantially degrading in many high latitude locations, resulting in
direct and indirect impacts on natural systems as well as human activities and infrastructure (Schuur et al., 2015; UNEP, 2012).
Coastal erosion is prevalent along the Western North American Arctic coastline and Eastern Siberia, and is one of the major
permafrost degradation processes (Lantuit et al., 2012). Coastal erosion mobilizes large amounts of sediment, organic matter
10 and nutrients from permafrost (Lantuit et al., 2012; Overduin et al., 2014; Retamal et al., 2008; Wegner et al., 2015) that are
released into the nearshore waters and affecting marine ecosystems (Bell et al., 2016; Dunton et al., 2006; Fritz et al., 2017).
At a number of locations, coastal erosion has been reported to be accelerating (Barnhart et al., 2014; Günther et al., 2013a;
Jones et al., 2008, 2009b; Mars and Houseknecht, 2007; Radosavljevic et al., 2016) but the current spatio-temporal resolution
of circum-arctic studies limits inferences of wide-spread changes in erosion rates (Fritz et al., 2017). The majority of permafrost
15 erosion studies compare multi-annual coastline changes to infer annualised erosion rates over periods of several years (Irrgang
et al., 2018; Overduin et al., 2014). However, such coarse observation frequencies neglect the intra-seasonal dynamics
including episodic thaw and abrupt erosion events during the open water season, knowledge of which is essential to understand
the mechanistic processes leading to rapid coastal erosion (Obu et al., 2016). Erosion plays a critical role in the longer-term
evolution of permafrost coastlines (Barnhart et al., 2014) and biogeochemical cycling in coastal zones (Fritz et al., 2017;
20 Semiletov et al., 2016; Vonk et al., 2012), and improved understanding of the drivers of coastal erosion are required to better
project future erosion rates with Arctic change.

Changes in permafrost landscapes are commonly measured using remote sensing. However, optical image coverage in high
latitude regions has historically been widely limited to relatively coarse temporal and spatial resolutions, due to frequent cloud
25 cover and logistical challenges that limit both satellite observations and aerial surveys (Hope et al., 2004; Stow et al., 2004).
Recently there has been a widespread interest in the use of lightweight drones, also known as remotely piloted aerial systems
or unmanned aerial vehicles (UAVs), to enable landscape managers and researchers to self-service their data collection needs
(Klemas, 2015; Westoby et al., 2012) thus democratizing data acquisition (DeBell et al., 2015). Over the last few years, drone
surveys are increasingly used for monitoring coastal systems (Casella et al., 2016; Duffy et al., 2017b; Mancini et al., 2013;
30 Turner et al., 2016). However, there have been very few examples of their application to monitor the ongoing rapid changes
along permafrost coastlines (although see Whalen, 2017; Whalen et al., 2017). Lightweight drones combined with image-
based modelling can provide highly accurate and detailed measurements of rapidly changing permafrost coastlines. These



aerial observations can be obtained at user-determined frequencies (e.g. weekly, daily, or even hourly if weather conditions permit), using relatively inexpensive tools as suitable multirotor drones are available for <\$1,500 USD. Information products include geolocated orthomosaics and digital surface models at temporal resolutions not available from more traditional forms of remote sensing (Casella et al., 2016; Stow et al., 2004; Whalen et al., 2017).

5

In this study, we used repeat drone surveys to investigate short-term dynamics of an eroding permafrost coastline at Qikiqtaruk – Herschel Island (Yukon Territory) in the Canadian Beaufort Sea across a 13-month period. We investigated what additional insights are available from observing shoreline positions at finer spatial and temporal grain, whether fine-grain observations of shoreline change could be related to meteorological and oceanographic variables, and compared intra-seasonal shoreline change with historical shoreline changes over the last 65 years. We demonstrated that lightweight drones and aerial photogrammetry can be cost effective tools to capture short-term coastal erosion dynamics and related shoreline changes along discrete sections of permafrost coasts. For our study area, we hypothesize that the erosion of the observed permafrost coastline adjacent to the settlement on Qikiqtaruk – Herschel Island varies greatly between years and continuing erosion could threaten key infrastructure to human activities on the island.

15 2 Study Area

Qikiqtaruk – Herschel Island is located in the western Canadian Arctic in the Beaufort Sea (69°N, 139°W, see supplementary figure S1). The island is an ice-thrust push-moraine formed during the maximal advance of the Laurentide ice sheet (Fritz et al., 2012; Pollard, 1990), and is underlain by ice-rich continuous permafrost (Brown et al., 1997; Lantuit and Pollard, 2008; Obu et al., 2016). Low spits composed of coarse material occur on the east and west sides of the island (Couture et al., 2018). Mean annual air temperature is -11°C (1970-2000) and mean annual precipitation is ca. 200 mm a⁻¹ (Burn, 2012). The average coastal erosion rate for the whole of Qikiqtaruk – Herschel Island was 0.45 m a⁻¹ between 1970 and 2000 (Lantuit and Pollard, 2005; Obu et al., 2015), and 0.68 m a⁻¹ between 2000-2011 (Obu et al., 2016).

Ice-breakup in this region typically commences in late June and open water conditions persist until early October (Dunton et al., 2006; Galley et al., 2016). For Herschel Basin and Thetis Bay, land-fast sea ice can be persistent for longer periods. The continental shelf at this part of the Beaufort Sea is very narrow and intersected by a deeper sea canyon, the Mackenzie Trough located north of Qikiqtaruk – Herschel Island (Dunton et al., 2006) (Figure 1b). The study area is characterised by dominant northwest (NW) and prevailing east (E) winds. Winds exert a strong influence on the wave and tide regime, and with easterly winds facilitating the transport of warm water from the Mackenzie River to Qikiqtaruk Herschel Island (Dunton et al., 2006). The interaction between meteorological factors including wind and wave action and coastal morphology exert more influence on water levels than tidal cycles in this microtidal setting (ca. 0.3-0.5 m range) (Huggett et al., 1975). North-westerly winds drive a positive storm surge and easterly winds drive a negative surge at Qikiqtaruk – Herschel Island (Héquette et al., 1995;

30



Héquette and Barnes, 1990). The contemporary rate of relative sea level rise along this part of the Canadian Beaufort Sea is thought to range between ca. 1.1 to 3.5 mm a⁻¹ (James et al., 2014; Manson et al., 2005).

This study focusses on a 500 m long coastal stretch located to the east of Kuvluraq – Simpson Point, a coarse clastic spit (Figure 1). The study stretch is along the edge of an alluvial fan, comprised of redeposited marine and glaciogenic sediments that form Qikiqtaruk – Herschel Island (Fritz et al., 2011; Rampton, 1982). The spit is attached to the alluvial fan, and is supplied by sediment from the alluvial fan and the high bluffs to the east (Radosavljevic et al., 2016). The focal coastline is characterized by low to moderately high bluffs (ca. 0.5 – 5 m in elevation). Ice contents in these bluffs are high, at ca. 40% ice by volume (Obu et al., 2016), although this value is slightly lower than the 50-60% ice content modelled for ice-thrust moraines along this portion of the Yukon Coast (Couture and Pollard, 2017). Permafrost temperatures are approximately -8°C (Burn and Zhang, 2009), and are known to be warming in recent decades (Burn and Zhang, 2009; Myers-Smith et al., Accepted). This study area lies entirely within the slightly larger ‘Coastal Reach 3’ unit considered by Radosavljevic *et al.* (2016), who reported coastal retreat rates of 1.4 ± 0.6 m a⁻¹, 1.7 ± 0.7 m a⁻¹ and 4.0 ± 1.1 m a⁻¹ for the periods 1952-1970, 1970-2000 and 2000-2011, respectively. For further details on the changing ecological and erosional context of this site, see Burn (2012), Radosavljevic *et al.* (2016) and Myers-Smith *et al.* (Accepted).

Coastal erosion at our study site threatens the human settlement and infrastructure on Qikiqtaruk – Herschel Island, located on Kuvluraq – Simpson Point (Olynyk, 2012; Radosavljevic et al., 2016). This gravel spit bounds the natural anchorage of Ilutaq – Pauline Cove, and is an important regional hub for local and indigenous travellers, park administration and rangers, tourists, and researchers in the western Canadian Arctic (e.g. Burn and Zhang, 2009; Myers-Smith et al., Accepted). The currently seasonally-inhabited settlement is part of the Qikiqtaruk – Herschel Island Territorial Park, and accommodates a number of culturally and historically significant sites resulting in its candidature for UNESCO World Heritage status (UNESCO, 2004). The proximity to the sea and low elevation of this settlement at ≤ 1.2 m above sea level leads to high risk of coastal hazards, particularly flooding (Myers-Smith and Lehtonen, 2016; Olynyk, 2012; Radosavljevic et al., 2016).

25 3 Methods

3.1 UAV image acquisition

In 2016, one drone survey was conducted in late July, followed by seven additional drone surveys over a 40-day period between July 6th and August 15th 2017. Drone surveys were conducted using two platforms: (i) a lightweight flying-wing Zeta Phantom FX-61 with a PixHawk flight controller equipped with a Sony RX-100ii camera (1” CMOS sensor with 20.2 Megapixels), and (ii) a multi-rotor DJI Phantom 4 Pro (1” CMOS sensor with 20 Megapixels). Drone operations were conducted in accordance with an SFOC issued by Transport Canada (to assist others seeking such permission, our full application is available at <https://arcticdrones.org/regulations/>). Artificial ground control markers were deployed along the shoreline and precisely



geolocated to an absolute accuracy of centimetres using global navigation satellite system (GNSS) equipment (Leica Geosystems). Image overlap, a function of front-lap and side-lap, captured each part of the study area in at least five and usually >10 photographs. Image overlap of five and 10 photos equates to fore-/side-lap values of 56% and 69%, respectively. For 2D orthomosaics and 3D elevation models, we would recommend aiming for ca. 8-10 and ca. 12-20 overlapping images
5 respectively. Drone surveys over this study area had flight times of ca. 15-25 minutes. The geotagged RGB photographs from each aerial survey had ground-sampling distances ranging from 10 mm to 40 mm. Although this study presents drone surveys for a limited (500 m) extent of shoreline, drone surveys could be optimised to observe larger reaches of up to ca. 1.5 to 2 km, particularly in jurisdictions such as Canada where current regulations permit UAV operations up to 0.5 nautical miles (926 m) from the remote pilot. For example, we found it possible to survey over eight km² in a single day with two drones operated by
10 two remote pilots. For further discussion of drone survey parameters for different applications, see Carrivick *et al.* (2016) and Duffy *et al.* (2017a).

3.2 Image alignment, shoreline mapping and shoreline analysis

Drone images were processed with structure-from-motion photogrammetry techniques, using Agisoft PhotoScan (version 1.3.3) (Agisoft, 2018; Sona *et al.*, 2014), and processing parameters reported in Table S1. GNSS-derived geolocations for each
15 individual image and precisely geolocated ground control markers provided additional spatial constraint of the photogrammetric processing (Carrivick *et al.*, 2016; Cunliffe *et al.*, 2016; Westoby *et al.*, 2012). This processing yielded georegistered orthomosaic composite images and digital surface models. Note that the heightfield approaches to surface modelling used in this analysis are not capable of capturing topographic change related to undercutting of bluffs. Capturing such overhanging features with photogrammetric methods can be possible, but requires optimising image acquisition and more
20 computationally intensive post-processing.

In addition to the drone surveys, we also used four ‘historic’ panchromatic aerial photographs from 1952 and 1970, and satellite images from 2000 and 2011 (previously analysed by Radosavljevic *et al.*, 2016). These four images had already been orthorectified in PCI Orthoengine to minimise image distortion. We co-registered these four ‘historic’ orthorectified images
25 to the 2017-07-06 orthomosaic image in a geographic information system (ArcGIS, version 10.5, ESRI), as we considered this orthomosaic to have the best spatial constraint and coverage of the seven drone datasets. The (composite) images from all twelve surveys were aligned to a common spatial framework, NAD83 UTM 7N (EPSG: 26907). Alignment errors estimated as the root mean square error (RMSE) of the control points. Further details of all images and composite orthomosaics are summarised in Table 1. While this approach to quantifying alignment error is standard practice in shoreline change analysis
30 (Irrgang *et al.*, 2018; Río and Gracia, 2013), we note that the RMSE of control points is not a strong metric of this uncertainty, as both transformation parameters (georeferencing) and the intrinsic and extrinsic camera parameters (structure-from-motion photogrammetry) are adjusted to optimise the RMSE of control points. Consequently, for an independent assessment of image registration error, it would be preferable to use the RMSE of *independent* check points, which were not used to constrain



transformation or bundle adjustment parameters (James et al., 2017). Visual comparison of each dataset indicated excellent spatial agreement and suitability for further analysis, in spite of different image acquisitions (Jones et al., 2018). Pixel error refers to the spatial grain of the digital satellite and orthomosaic composite images, and is a metric of image quality calculated for aerial photographs based on the scale factor of each image multiplied by the typical resolution of a 9 x 9-in aerial photogrammetric camera (after Radosavljevic et al., 2016).

The shorelines of all twelve images were digitised manually in ArcGIS, at a scale of 1:600 for the four, older, coarse-grained panchromatic images, and a scale of 1:80 for the eight, fine-grained red-green-blue (RGB) orthomosaics. The shoreline was defined as the vegetation edge, which is generally the preferred shoreline proxy, rather than the wet-dry line previously used in this region (Radosavljevic et al., 2016), because the vegetation edge was both more visually distinct and temporally consistent than the wet-dry line (Boak and Turner, 2005). Temporal consistency was essential to ensure meaningful assessment of rapid coastal retreat over short time intervals (Río and Gracia, 2013). Shoreline digitising errors were derived from the estimated accuracy of operator vegetation edge detection, informed by reference to finer grain aerial imagery. Mapping shoreline edges was possible with much greater fidelity using the fine spatial grain RGB orthomosaic images compared to the coarser-grained panchromatic images, where low contrast was sometimes an issue (Boak and Turner, 2005; Río and Gracia, 2013). These differences contributed to the estimated digitising errors, which contribute towards the overall uncertainty estimates (Table 1).

Total shoreline uncertainties were calculated as the sum of georeferencing, pixel and digitising errors (Radosavljevic et al., 2016; Río and Gracia, 2013), and survey parameters and shoreline errors are given in Table 1. Shoreline position statistics were calculated with the USGS Digital Shoreline Analysis System (DSAS) extension for ArcGIS (Thieler et al., 2009), using the same baseline and shore normal transects at 5 m intervals as used by Radosavljevic *et al.* (2016). Shoreline retreat rates in this study are given in end point rates for comparison between surveys, and both end point rate and linear regression rate for the entire time period of the study. The linear regression rate uncertainty is the standard error of the slope of at the 95% confidence interval. For further discussion on erosion rate calculation, see Thieler *et al.* (2009). The accuracy of calculated shoreline change rates was calculated as the dilution of accuracy (DOA) (Dolan et al., 1991; Irrgang et al., 2018), as shown in Equation 1:

$$DOA = \frac{\sqrt{U_i^2 + U_{ii}^2}}{\Delta t} \quad (\text{Equation. 1})$$

Where U_i is the total shoreline uncertainty of the first point in time (from Table 1), U_{ii} is the total shoreline uncertainty of the shoreline position from the second point in time, and Δt is the duration of the time period in years or days, as appropriate. Table 2 displays the DOAs for all analysed time periods. Erosion rate errors refer to DOA values, unless otherwise stated.



3.3. Meteorological and oceanographic observations

Meteorological observations were obtained from an Environment Canada weather station located on Kuvluraq – Simpson Point (station ID: ‘Herschel Island - Yukon Territory’, World Meteorological Organisation ID: 71501; downloaded from http://climate.weather.gc.ca/climate_data_on_2018-01-03). Mean 6-hour air temperature, wind speed, and wind direction throughout the 2017 observation period are displayed in Figure 5, and general wind conditions are summarised in Figure S1 and Radosavljevic *et al.* (2016). Conductivity-temperature-depth (CTD) profiles (see supporting figure S2) were collected in July and August 2015 with a CastAway CTD (SonTek, USA) from a small research vessel ca. 1 km from the study area (near to 69.552°N, 138.923°W). To inform qualitative interpretation of the erosion dynamics at this location, a time-lapse camera was installed at the location indicated on Figure 1 between 2017-07-29 and 2017-08-03.

10 4 Results

4.1. Shoreline position analysis

Over our observational record from 1952 to 2017, the coastline along the study reach retreated by a net total of 143.7 ± 28.4 m (where \pm is the standard deviation of observations from each transect). The overall retreat rate was 2.2 ± 0.2 m a⁻¹ as calculated by end-point rate, and 1.9 ± 0.5 m a⁻¹ as calculated by the linear regression rate. Average retreat rates over decadal periods ranged between 0.7 ± 0.5 m a⁻¹ to 3.0 ± 0.8 m a⁻¹. Table 2 presents the net shoreline change and end-point rates for all periods.

Over a 40-day period in the summer of 2017, shoreline retreat was 14.5 ± 3.2 m, an average rate of 36 cm per day. The shoreline position during different drone surveys are illustrated in Figures 2 and 3. The high temporal frequency of observations throughout the summer of 2017 and the highly episodic nature of coastal retreat meant that shorelines were sometimes very close in space, as illustrated in Figure 2a and 2b, Figure 3. Coastline retreat was highly episodic in time and space, occurring primarily over two periods: (i) 27 days between July 13th to July 30th and (ii) four days between August 11th to August 15th (Figures 2, 3, and 5, Table 2). There was minimal change in coastline position between August 5th and August 11th, the seven days between July 6th to July 13th, and the six days between July 30th and August 5th (Figure 2, Table 2).

4.2. Digital elevation profiles

Digital surface models of the coastal topography were generated from the photogrammetric surveys undertaken in 2016 and 2017, spanning a 13 month period. Cross-sectional profiles through these digital surface models across a ca. 3 m high bluff are shown in Figure 4, sampled across the A-B-transect indicated on Figure 3. The depression in the 2017-08-15 elevation profile corresponds with the ca. 1 m gap behind a detached block, depicted in Figure 3c.



4.3. Meteorological, oceanographic and time-lapse video observations

Erosion rates for each observation period through the summer of 2017 were compared to meteorological and oceanographic conditions, in order to better describe the controls on episodic and rapid erosion of this coastline. From three to 10 days prior to the first 2017 survey (on 2017-07-06), winds were consistently strong from the east and reached up to 40 km h^{-1} (Figure 5).

5 For zero to three days prior to the 1st 2017 survey (on 2017-07-06) the dominant wind direction shifted to the northwest with strong winds up to 40 km h^{-1} (Figure 5), which raised the water level and refracted waves around the bluffs at Collinson Head to the northeast of the study reach. Over the seven days between the 6th and 13th of July 2017, winds were predominantly from the southeast, with brief periods of high strength winds (ca. 30 km h^{-1} over six hours) from the northwest (Figure 5). These meteorological conditions generally promoted waves from the southeast, which attacked the exposed cliff base (Figures 4 and

10 5). Over the 17 days between the 13th and 30th of July, winds were variable, but predominantly from the southeast, with two notable periods of very high strength winds (ca. 40 km h^{-1} for 24 and 12 hours, respectively) (Figure 5), and surface water temperatures reached nearly 10°C (see Fig. S3, CTD profile d). These conditions combined to drive rapid erosion resulting in $7.4 \pm 5.6 \text{ m}$ (SD) of shoreline retreat in just 17 days (Figures 3 and 4).

15 Over the six days between the 30th of July to the 5th of August, winds were variable in direction and typically weaker (Figure 5). This resulted in minimal shoreline retreat (Table 2), but did remove cliff debris from the beach (video S1, Figure 4) and facilitating further undercutting. Over the six days between the 5th to the 11th of August, the wind direction was variable and wind speed low (mostly below 20 km h^{-1}), with relatively slow coastline retreat of ca. 0.17 m d^{-1} . Over the four days between the 11th and 15th of August, a larger storm event developed, with wind shifting from east through north to west and wind speeds

20 increasing to excess of 45 km h^{-1} for >6 hours (Figure 5). These meteorological conditions resulted in undercutting and large waves that caused $4.1 \pm 1.1 \text{ m}$ (SD) of shoreline retreat in just four days, largely through block failure (Figures 3, 4 and S4, Table 2). Sea surface temperatures were relatively warm at $6\text{-}10^\circ\text{C}$ when measured between the 21st of July and the 2nd of August (Figure 5, Figure S2). Figure S1 summarises wind vectors and velocities observed during the summer of 2017. A time-lapse video illustrating the erosion at this coastline over five days from the location marked in Figure 1 is presented in video

25 S1.

5. Discussion

Over the 65-year record, we consistently observe substantial erosion along the focal coastline on Qikiqtaruk – Herschel Island. This part of the coast retreated on average by 2.2 m a^{-1} , which is fast relative to the spatially weighted means of 1.1 m a^{-1} for the Canadian Beaufort Sea and 0.57 m a^{-1} for the circum-Arctic (Lantuit et al., 2012) where retreat rates typically ranges

30 between $0\text{-}2 \text{ m a}^{-1}$ (Overduin et al., 2014). Shoreline retreat varied substantially throughout the 65-year period (Radosavljevic et al., 2016). In 2017, we observed 14.5 m of coastline retreat within a single year, which exceeds the long-term average retreat



of 2.2 m a⁻¹ by more than a factor of six. The potential factors driving this rapid retreat are discussed below, and include both long-term pre-conditioning factors over timescales of years to decades and short-term factors over timescales of days to weeks.

5.1. The advantages and disadvantages of using drones to quantify short-term coastal erosion dynamics

5 The use of drone surveys in this study proved to be an effective tool to measure the dynamics of short-term erosion along this permafrost coastline. Photogrammetric analysis of drone-acquired image data yielded orthomosaics, inferred shoreline positions (Figures 3 and 4), and elevation models (Figure 4) that provide quantitative information on coastal structure. Drone surveys can provide fine spatial grain and accurate measurements of the coastline position at high temporal frequencies, allowing coastline change to be quantified and related to meteorological observations on a supra-annual timescale (Figure 5).
10 Over a 384-day period from July 2016 to August 2017, we were able to observe a very rapid and substantial change in the shoreline position using drone surveys, on average 17.4 m of retreat across the 500 m study reach. Given the episodic nature of coastal retreat, it is difficult to compare short-term rate changes with long-term observation periods (<2 vs. >10 years, respectively) (Dolan et al., 1991). In this case, however, for the total 17.4 m of shoreline retreat between 2016 and 2017 reported here to remain consistent with the long-term average of 2.2 m a⁻¹, no further erosion of this reach would need to occur
15 for more than seven years.

Lightweight drones can be deployed at relatively low cost when suitably trained and equipped personnel are on-site. However, the costs of accessing high latitude sites can be substantial, potentially contributing to uneven distributions of monitoring sites (Metcalf et al., 2018). The temporal resolution of drone surveys can greatly exceed those available by more traditional forms
20 of remote sensing, for example satellite observations or surveys from manned aircraft (Casella et al., 2016; Stow et al., 2004; Whalen et al., 2017). High temporal frequency surveys can provide quantitative insights into erosion processes that vary greatly in time and space, and these quantitative measurements may have stronger physical meaning than previously available proxies, such as the apparent cross sectional area of detached blocks extracted from time-lapse photography (e.g. Barnhart et al., 2014). Surveyable spatial extents are also limited by safety and regulatory restrictions, and depend on the size and the range of the
25 remotely piloted drone. When supplemented by other monitoring of environmental variables (such as wave field and sea surface temperature), such spatial observations could be used to robustly evaluate and subsequently refine process-based numerical models of coastal erosion over multiple temporal scales (Barnhart et al., 2014; Casella et al., 2014; Wobus et al., 2011).

30 By allowing measurement of the volume and consequently mass of eroded material, digital elevation models can be more informative than simple 2D representations of shoreline position. Digital elevation models were generated following the eight drone surveys (Figure 4). However, faster than anticipated coastal retreat destroyed some ground control markers, resulting in



insufficient spatial constraint of the photogrammetric reconstructions of two of the latter surveys (2017-08-05 and 2017-08-15). This weaker constraint contributed to larger elevation errors in these two reconstructions, resulting in the apparent datum shift in Figure 4. If 3D elevation observations are required, care should be taken when deploying ground control markers and conducting drone surveys to ensure that there will be sufficient spatial constraint of the photogrammetric modelling process, even if coastal retreat is faster than expected. For further recommendations on optimising ground control placement, see Carrivick *et al.* (2016) and James *et al.* (2017).

In summary, drone surveys are highly suitable when there is a need to accurately measure small changes (e.g. ≤ 0.3 m) in shoreline positions over limited extents (e.g. ≤ 5 -10 km in length). Fine spatial grain measurements from drone products are especially useful for isolating the drivers of coastal erosion events, and continued miniaturization of thermal and multispectral cameras for drone platforms will create opportunities to better understand these mechanisms of change. While drone surveys can also be used when shoreline position changes are much greater, traditional data sources such as optical satellite observations can be better suited for observing change across larger sections of coastline. High levels of cloud cover in Arctic regions limits the frequency of successful observations (Hope *et al.*, 2004; Stow *et al.*, 2004), but continuing advances in satellite sensors have increased the spatial resolution and revisit frequency of observations. Despite this, freely available products are currently only available for spatial grains of ca. ≥ 10 m (e.g. Sentinel 2), and finer-grain (< 4 m) products have non-trivial costs for each scene.

5.2. Short-term coastal erosion dynamics

Between the survey in 2016 (2016-07-26) and the first survey in 2017 (2017-07-06), a large portion of beach and cliff debris appeared to have been removed (Figure 4), potentially during storm events in the autumn of 2016 or ice bulldozing during ice-breakup in spring 2017. Removal of this protective material may have increased the susceptibility of these cliffs to rapid erosion in the summer of 2017. The two periods with the most rapid erosion in 2017 (the 27 days between July 13th to July 30th, and the four days between August 11th to August 15th) were both associated with strong wind events (six-hour moving averages exceeding >40 km h⁻¹) preceded by relatively high air and water temperatures. Together, these conditions likely enhanced the thermo-abrasional processes undercutting the ice-rich bluff prior to the first survey, creating the conditions for abrupt erosion. Further work relating coastline change to meteorological and oceanographic factors over short timescales would need to further consider the latencies involved between meteorological and oceanographic conditions, undercutting of permafrost cliffs, and planform change as observed from an aerial perspective.

The coastal erosion processes we observed during 40 days of 2017 correspond with the conceptual model described by Barnhart *et al.* (2014) (Video S1 and Figure S3). The bluffs along the alluvial fan were affected by both thermo-denudation but particularly thermo-abrasion due to the combined mechanical and thermal action of sea water causing undercutting and



subsequent block failure (Barnhart et al., 2014; Günther et al., 2012). These thermal processes are likely influenced by warm surface waters delivered from the Mackenzie River Delta during easterly wind conditions (Dunton et al., 2006). Further factors facilitating rapid erosion at this coastal reach is the high ice content (ca. 40% Obu et al., 2016) and the low relief, as less material is deposited at the base of the bluff following cliff failure, thus reducing protection of the bluff base from further wave action (Héquette and Barnes, 1990).

Over shorter timescales through the summer of 2017, coastal retreat was highly episodic. The main mode of erosion was block failure driven by thermo-abrasional undercutting, which appeared to be largely influenced by fluctuations in water level combined with wave action. Water level fluctuations appeared to be mainly determined by wind generated surges and waves, superimposed on tidal patterns. Although this region is microtidal, with a mean range of just 0.15 m for semidiurnal and monthly tides, these are superimposed on a ca. 0.66 m annual tidal cycle which peaks in late July (Barnhart et al., 2014), corresponding with our intensive short-term observation period. Annual tides may influence the timing of coastal retreat within the ice-free season in this area. Winds exert substantial control over local sea levels, with north-westerly winds driving a positive storm surge and easterly winds driving a negative storm surge (Héquette et al., 1995; Héquette and Barnes, 1990). The direction and frequency of wind patterns observed in 2017 (Figure 5, Figure S1) are similar to those reported in June-Sept from 2009 to 2012 (Radosavljevic et al., 2016 figure 4 therein). However, overall wind speeds were higher in 2017, with a greater proportion of periods with mean speeds in excess of $>30 \text{ km h}^{-1}$. During the two periods with highest erosion rates, there were multiple strong storm events with both easterly and north-westerly winds with 6-hour average speeds in excess of 30 km h^{-1} and 40 km h^{-1} , respectively (Figure 5). We were able to provide quantitative insights into these highly episodic erosion processes, because of the high temporal frequency of shoreline position observations. For example, ca. 30% (4.2 m) of the 14.5 m of shoreline retreat occurring in the summer of 2017 happened in just four days (August 11th to August 15th), suggesting that discrete storm events can play a major role in permafrost shoreline evolution (Solomon et al., 1993).

5.3 Long-term pre-conditioning of coastal erosion

Our observations suggest that the rapid coastal retreat in 2017 may have resulted from multiple factors interacting over several years. On Qikiqtaruk – Herschel Island, atmospheric warming (Burn and Zhang, 2009; Myers-Smith et al., Accepted) has increased the temperature of permafrost (Burn and Zhang, 2009; Myers-Smith et al., Accepted) and deepened the active layer (Myers-Smith et al., Accepted) at locations ca. 1 km from the study reach. Permafrost temperatures along the study reach are likely also be influenced by a creek, which discharges across parts of the alluvial fan (Figure 1); however, long-term discharge records do not exist for this stream. In this area, the onset of seasonal sea-ice melt has moved earlier over the last 18 years, with ice-free seasons lengthening by 9 days per decade between 1979-2013 (Stroeve et al., 2014), and decreasing summer minimum sea ice concentrations over the last 39 years (Myers-Smith et al., Accepted). The combination of relative sea level rise of 1.1 to 3.5 mm a^{-1} (James et al., 2014; Manson et al., 2005), earlier ice-break up (Mahoney et al., 2014) and longer open



water seasons (Barnhart et al., 2014; Stroeve et al., 2014), increased wave heights (Barnhart et al., 2014), and increased transport of warm water discharged from the nearby Mackenzie River (Carmack and Macdonald, 2002; Dunton et al., 2006; van Vliet et al., 2013) are long-term factors which likely enhance the thermo-abrasion of permafrost bluffs at this site.

5 5.4. Short-term coastal erosion in the context of long-term observations

The overall rapid coastline retreat observed in this study reach is consistent with, but greater than, earlier analysis of neighbouring coastal reaches on Qikiqtaruk – Herschel Island between 1952 and 2011 (Radosavljevic et al., 2016) and also coastal retreat observed in other Arctic permafrost coastlines (Günther et al., 2013b; Irrgang et al., 2018; Jones et al., 2009a; Whalen et al., 2017). Coastline retreat rates almost doubled from 7.6 m a⁻¹ (1955-2009) to 13.8 m a⁻¹ (2007-2009) at Cape Halkett on the Alaskan Beaufort Sea (Jones et al., 2009a), and more than doubled from 2.2 m a⁻¹ (1952-2010) to 5.3 m a⁻¹ (2010-2012) on Bykovsky Island, Siberia (Günther et al., 2013b). Increases in erosion rates greater than two-fold are generally reported for low elevation coasts, such as the one shown in this paper and in (Jones et al., 2009a). On the Yukon Coast, average coastal retreat rates were 0.5 m a⁻¹ between 1950-1970 (Harper et al., 1985) and 0.7 m a⁻¹ between 1950-2011 (Irrgang et al., 2018), with maximum reported rates of 22 m a⁻¹ on Pelly Island (NWT) 130 km to the east along the Yukon-NWT Coast (Whalen et al., 2017). Robustly testing whether erosion of permafrost coastlines may be accelerating in this region and more widely will require further analysis of shoreline position change at (near-)annual temporal resolution, considering a larger range of representative coastal reaches and study sites.

Over the 65 years from 1952 to 2017, the coastline in this study reach retreated at a rate of 2.2 m a⁻¹, with average rates over decadal periods ranging between 0.7 to 3.0 m a⁻¹ (Table 2). This study reach lies within the slightly larger ‘coastal reach 3’ unit considered by Radosavljevic *et al.* (2016); consequently, differences in reach length and historic image co-registration result in some slight differences between the erosion rates reported herein and those previously reported. Our finding that the overall retreat rate calculated from the linear regression method (1.9 m a⁻¹) is more conservative than the rate calculated by the end-point method (2.2 m a⁻¹) is consistent with earlier reports (Radosavljevic et al., 2016). In either case, this long-term rate is fast relative to circum-arctic observations, where retreat rates are typically between 0-2 m a⁻¹ (Overduin et al., 2014), with a weighted mean of 0.57 m a⁻¹ for the entire Arctic, 1.1 m a⁻¹ for the Canadian Beaufort Sea (Lantuit et al., 2012), and 0.7 m a⁻¹ for the Yukon coast (Irrgang et al., 2018). Coastal retreat rates in the neighbouring Alaskan Beaufort Sea were typically 0.7 to 2.4 m a⁻¹ depending on coast type (Jorgenson and Brown, 2005), with extremes of up to 25 m a⁻¹ (Jones et al., 2009b). Yet, the Alaskan Beaufort Sea coastline is more similar to the western formerly non-glaciated part of the Yukon Coast, with low cliffs, overall strong erosion rates and longer sea ice cover (Irrgang et al., 2018; Jorgenson and Brown, 2005; Ping et al., 2011). This is quite different from our study coastline in the formerly glaciated part of the Yukon Coast (Rampton, 1982), which is characterised by high cliffs and high ground ice contents due to former movement and burial of glacier ice (Couture and Pollard, 2017; Fritz et al., 2011). Furthermore, the sea-ice free season in our study area is longer than further west along the



Alaska Coast due to the warming influence of the Mackenzie River, but in turn is modulated by the breakup of land-fast ice, which can be persistent in Herschel Basin and Thetis Bay (Dunton et al., 2006).

5.5. Rapid coastal erosion as potential threat for the Territorial Parks infrastructure

Coastal change in this area influences the stability and evolution of the spit, which accommodates culturally and historically significant sites, as well as infrastructure essential to the operation of the Qikiqtaruk – Herschel Island Territorial Park. Shoreline change and flooding in recent history has necessitated the relocation and raising of several historic buildings at Ilutaq – Pauline Cove, as well as the relocation of the gravel airstrip essential to the operation of the Park (Olynyk, 2012). However relocation efforts are hindered by the fragility of several buildings, particularly the ‘Community House’, the oldest building in the Yukon, and it is increasingly difficult to find safer locations for these buildings on the spit (Olynyk, 2012). These historic buildings underpin the site’s candidature for UNESCO status (UNESCO, 2004). Erosion of the observed coastal reach adjacent to the settlement exposes the base of the spit to coastal processes, and increases the risk of changes to the position of the spit itself. Flooding during storm events has already been observed to cut off the spit from the island (Myers-Smith and Lehtonen, 2016), and these events are projected to become more common in the future (Radosavljevic et al., 2016). Knowledge of coastal processes, particularly patterns of contemporary coastal retreat as a proxy for future patterns, is therefore critical for informing the management of Qikiqtaruk – Herschel Island Park.

6. Conclusion

We used drones as a highly effective instrument to observe the dynamics of permafrost coastline changes associated with supra-seasonal erosion on Qikiqtaruk – Herschel Island. In 2017, average shoreline retreat was extremely rapid at 14.5 m, well in excess of the long-term average of 2.2 m a⁻¹ from 1952 to 2017. Thirty percent of the 2017 change in shoreline position (4.1 m) occurred in just 4 days during one storm event. Block failure was the prevailing mode of erosion, seemingly driven by multiple factors that increase the susceptibility of the permafrost coastline to thermo-abrasional processes. These rapid erosion events observed on Qikiqtaruk – Herschel Island appear to have been driven by short-term fluctuations in water levels due to meteorological conditions, possibly superimposed on annual tidal cycles, on a longer-term background of relative sea level rise and increasing heat flux from the Mackenzie River discharge and the atmosphere.

At our study site on Qikiqtaruk – Herschel Island further erosion and removal of this coastal reach could threaten the infrastructure of the settlement over the long-term. With the rapid maturation of drone platforms and image-based modelling technologies, these approaches can now be easily deployed at both supra and sub-annual timescales to obtain new insights into coastal erosion and inform management decisions. These approaches are particularly relevant in permafrost coastlines, where erosion is highly episodic, with long-term rates dominated by short-term events. By combining new methods of observation



with long-term records, we can improve predictions of coastal erosion dynamics and subsequent consequences for the management of fragile Arctic coastal ecosystems and cultural sites.

Acknowledgements

This work was made possible by support from NERC (ShrubTundra - NE/M016323/1), the loan of GNSS equipment from
5 NERC Geophysical Equipment Facility (GEF:1063 and 1069), the National Geographic Society (Grant CP-061R-17), and the
Helmholtz Young Investigators Group ‘COPER’ (grant #VH-NG-801). This study was supported by funding from the
European Union’s Horizon 2020 research and innovation programme (Nunataryuk - grant #773421). Drone flight operations
were authorised by a Special Flight Operations Certificate granted by Transport Canada. We wish to thank the Qikiqtaruk
Territorial Park staff including Richard Gordon, Edward McLeod, Samuel McLeod, Ricky Joe, Paden Lennie, and Shane
10 Goesen, as well as the Yukon Government and Yukon Parks for their permission and support of this research (Permit number
Inu-02-16). We also thank the Inuvialuit people for their permission to work on their traditional lands. We thank James Duffy,
and anonymous reviewers for insightful feedback that helped us to refine earlier versions of this manuscript.

Statement of Contribution

Conceptualization, AC, GT, JK and IM-S; Data curation, AC; Formal analysis, AC and GT; Funding acquisition, IM-S, TS,
15 and HL; Investigation, AC, GT, BR, WP and JK; Methodology, AC; Project administration, AC; Supervision, TS, HL and IM-
S; Visualization, AC, GT and WP; Writing – original draft, AC; Writing – review & editing, AC, GT, BR, WP, TS, HL, JK
and IM-S.

Conflicts of Interest

The authors declare that they have no conflict of interest. The funding sponsors had no role in the design of the study; in the
20 collection, analyses, or interpretation of data; in the writing of the manuscript, or in the decision to publish the results.

References

- Agisoft: Agisoft PhotoScan User Manual: Professional Edition, V 1.4, Agisoft., 2018.
- Barnhart, K. R., Anderson, R. S., Overeem, I., Wobus, C., Clow, G. D., Gary D. Clow, and Urban, F. E.: Modeling erosion of
ice-rich permafrost bluffs along the Alaskan Beaufort Sea coast, *Journal of Geophysical Research: Earth Surface*,
25 doi:10.1002/2013JF002845, 2014.
- Bell, L. E., Bluhm, B. A. and Iken, K.: Influence of terrestrial organic matter in marine food webs of the Beaufort Sea shelf
and slope, *Marine Ecology Progress Series*, 550, 1–24, doi:10.3354/meps11725, 2016.



- Boak, E. H. and Turner, I. L.: Shoreline Definition and Detection: A Review, *Journal of Coastal Research*, 688–703, doi:10.2112/03-0071.1, 2005.
- Brown, J., Ferrians Jr., O. J., Heginbottom, J. A. and Melnikov, E. S.: Circum-Arctic map of permafrost and ground-ice conditions, USGS Numbered Series. [online] Available from: <http://pubs.er.usgs.gov/publication/cp45> (Accessed 9 April 2018), 1997.
- 5
- Burn, C. R.: *Herschel Island Qikiqtaryuk: A Natural and Cultural History of Yukon's Arctic Island*, 1st ed., Calgary University Press., 2012.
- Burn, C. R. and Zhang, Y.: Permafrost and climate change at Herschel Island (Qikiqtaruq), Yukon Territory, Canada, *J. Geophys. Res.*, 114(F2), F02001, doi:10.1029/2008JF001087, 2009.
- 10
- Carmack, E. C. and Macdonald, R. W.: *Oceanography of the Canadian Shelf of the Beaufort Sea: A Setting for Marine Life*, *ARCTIC*, 55(5), 29–45, doi:10.14430/arctic733, 2002.
- Carrivick, J. L., Smith, M. W. and Quincey, D. J.: *Structure from Motion in the Geosciences*, John Wiley & Sons, Ltd, Chichester, UK., 2016.
- Casella, E., Rovere, A., Pedroncini, A., Mucerino, L., Casella, M., Cusati, L. A., Vacchi, M., Ferrari, M. and Firpo, M.: Study of wave runup using numerical models and low-altitude aerial photogrammetry: A tool for coastal management, *Estuarine, Coastal and Shelf Science*, 149, 160–167, doi:10.1016/j.ecss.2014.08.012, 2014.
- 15
- Casella, E., Rovere, A., Pedroncini, A., Stark, C. P., Casella, M., Ferrari, M. and Firpo, M.: Drones as tools for monitoring beach topography changes in the Ligurian Sea (NW Mediterranean), *Geo-Mar Lett*, 36(2), 151–163, doi:10.1007/s00367-016-0435-9, 2016.
- 20
- Couture, N. J. and Pollard, W. H.: *A Model for Quantifying Ground-Ice Volume, Yukon Coast, Western Arctic Canada*, *Permafrost and Periglac. Process.*, 28(3), 534–542, doi:10.1002/ppp.1952, 2017.
- Couture, N. J., Irrgang, A., Pollard, W., Lantuit, H. and Fritz, M.: Coastal Erosion of Permafrost Soils Along the Yukon Coastal Plain and Fluxes of Organic Carbon to the Canadian Beaufort Sea, *J. Geophys. Res. Biogeosci.*, 2017JG004166, doi:10.1002/2017JG004166, 2018.
- 25
- Cunliffe, A. M., Brazier, R. E. and Anderson, K.: Ultra-fine grain landscape-scale quantification of dryland vegetation structure with drone-acquired structure-from-motion photogrammetry, *Remote Sensing of Environment*, 183, 129–143, doi:10.1016/j.rse.2016.05.019, 2016.
- DeBell, L., Anderson, K., Brazier, R. E., King, N. and Jones, L.: Water resource management at catchment scales using lightweight UAVs: current capabilities and future perspectives, *J. Unmanned Veh. Sys.*, doi:10.1139/juvs-2015-0026, 2015.
- 30
- Dolan, R., Fenster, M. S. and Holme, S. J.: Temporal analysis of shoreline recession and accretion, *Journal of Coastal Research*, 7(3), 723–744, 1991.
- Duffy, J. P., Cunliffe, A. M., DeBell, L., Sandbrook, C., Wich, S. A., Shutler, J. D., Myers-Smith, I. H., Varela, M. R. and Anderson, K.: Location, location, location: considerations when using lightweight drones in challenging environments, *Remote Sens Ecol Conserv*, doi:10.1002/rse2.58, 2017a.
- 35
- Duffy, J. P., Pratt, L., Anderson, K., Land, P. E. and Shutler, J. D.: Spatial assessment of intertidal seagrass meadows using optical imaging systems and a lightweight drone, *Estuarine, Coastal and Shelf Science*, doi:10.1016/j.ecss.2017.11.001, 2017b.



- Dunton, K. H., Weingartner, T. and Carmack, E. C.: The nearshore western Beaufort Sea ecosystem: Circulation and importance of terrestrial carbon in arctic coastal food webs, *Progress in Oceanography*, 71(2), 362–378, doi:10.1016/j.pocean.2006.09.011, 2006.
- Environment Canada: [online] Available from: http://climate.weather.gc.ca/climate_data (Accessed 3 January 2018), 2017.
- 5 ESRI, TerraColor and Earthstar Geographics: Basemap, [online] Available from: http://goto.arcgisonline.com/maps/Arctic_Imagery, 2018.
- Fritz, M., Wetterich, S., Meyer, H., Schirrmeister, L., Lantuit, H. and Pollard, W. H.: Origin and characteristics of massive ground ice on Herschel Island (western Canadian Arctic) as revealed by stable water isotope and Hydrochemical signatures, *Permafrost Periglac. Process.*, 22(1), 26–38, doi:10.1002/ppp.714, 2011.
- 10 Fritz, M., Wetterich, S., Schirrmeister, L., Meyer, H., Lantuit, H., Preusser, F. and Pollard, W. H.: Eastern Beringia and beyond: Late Wisconsinan and Holocene landscape dynamics along the Yukon Coastal Plain, Canada, *Palaeogeography, Palaeoclimatology, Palaeoecology*, 319–320, 28–45, doi:10.1016/j.palaeo.2011.12.015, 2012.
- Fritz, M., Vonk, J. E. and Lantuit, H.: Collapsing Arctic coastlines, *Nature Clim. Change*, 7(1), 6–7, doi:10.1038/nclimate3188, 2017.
- 15 Galley, R. J., Babb, D., Ogi, M., Else, B. G. T., Geilfus, N.-X., Crabeck, O., Barber, D. G. and Rysgaard, S.: Replacement of multiyear sea ice and changes in the open water season duration in the Beaufort Sea since 2004, *J. Geophys. Res. Oceans*, 121(3), 1806–1823, doi:10.1002/2015JC011583, 2016.
- Günther, F., Overduin, P. P., Sandakov, A., Grosse, G. and Grigoriev, M. N.: Thermo-erosion along the Yedoma coast of the Buor Khaya peninsula, Laptev Sea, East Siberia, in *Proceedings of the Tenth International Conference on Permafrost, Volume 1: International Contributions*, edited by K. Hinkel, pp. 137–142., 2012.
- 20 Günther, F., Overduin, P. P., Baranskaya, A., Opel, T. and Grigoriev, M. N.: Observing Muostakh Island disappear: erosion of a ground-ice-rich coast in response to summer warming and sea ice reduction on the East Siberian shelf, *Cryosphere Discussions*, 7(4), 4101–4176, doi:10.5194/tcd-7-4101-2013, 2013a.
- Günther, F., Overduin, P. P., Sandakov, A. V., Grosse, G. and Grigoriev, M. N.: Short- and long-term thermo-erosion of ice-rich permafrost coasts in the Laptev Sea region, *Biogeosciences*, 10(6), 4297–4318, doi:10.5194/bg-10-4297-2013, 2013b.
- 25 Harper, J. R., Reimer, P. D. and Collins, A. D.: Canadian Beaufort Sea physical shore-zone analysis, Report for Northern Oil and Gas Action Plan, Indian and Northern Affairs Canada Ottawa, Canada. [online] Available from: <http://engineerradcc.library.link/portal/Canadian-Beaufort-Sea-physical-shore-zone/Gu3YaBSD3Pk/>, 1985.
- Héquette, A. and Barnes, P. W.: Coastal retreat and shoreface profile variations in the Canadian Beaufort Sea, *Marine Geology*, 30 91(1), 113–132, doi:10.1016/0025-3227(90)90136-8, 1990.
- Héquette, A., Desrosiers, M. and Barnes, P. W.: Sea ice scouring on the inner shelf of the southeastern Canadian Beaufort Sea, *Marine Geology*, 128(3), 201–219, doi:10.1016/0025-3227(95)00095-G, 1995.
- Hope, A. S., Pence, K. R. and Stow, D. A.: NDVI from low altitude aircraft and composited NOAA AVHRR data for scaling Arctic ecosystem fluxes, *International Journal of Remote Sensing*, 25(20), 4237–4250, doi:10.1080/01431160310001632710, 35 2004.



- Huggett, W. S., Woodward, M. J., Stephenson, F., Hermiston, F. V. and Douglas, A.: Near and Bottom Currents and Offshore Tides, Ocean and Aquatic Sciences, Department of Environment., 1975.
- IPCC: Climate Change 2013: The Physical Science Basis. Contribution of Working Group I to the Fifth Assessment Report of the Intergovernmental Panel on Climate Change, edited by T. F. Stocker, D. Qin, G.-K. Plattner, M. M. B. Tignor, S. K. Allen, J. Boschung, A. Nauels, Y. Xia, V. Bex, and P. Midgley, p. 996, Cambridge University Press, Cambridge, United Kingdom., 2013.
- Irrgang, A. M., Lantuit, H., Manson, G. K., Günther, F., Grosse, G. and Overduin, P. P.: Variability in Rates of Coastal Change Along the Yukon Coast, 1951 to 2015, *Journal of Geophysical Research: Earth Surface*, 123(4), 779–800, doi:10.1002/2017JF004326, 2018.
- 10 James, M. R., Robson, S., d’Oleire-Oltmanns, S. and Niethammer, U.: Optimising UAV topographic surveys processed with structure-from-motion: Ground control quality, quantity and bundle adjustment, *Geomorphology*, 280, 51–66, doi:10.1016/j.geomorph.2016.11.021, 2017.
- James, T. S., Henton, J. A., Leonard, L. J., Darlington, A., Forbes, D. L. and Craymer, M.: Relative sea-level projections in Canada and the adjacent mainland United States, Geological Survey of Canada, Ottawa, Ontario. [online] Available from: Retrieved from http://ftp2.cits.rncan.gc.ca/pub/geott/ess_pubs/295/295574/of_7737.pdf, 2014.
- 15 Jones, B. M., Hinkel, K. M., Arp, C. D. and Eisner, W. R.: Modern erosion rates and loss of coastal features and sites, Beaufort Sea coastline, Alaska, Arctic, 61(4), 12, 2008.
- Jones, B. M., Arp, C. D., Beck, R. A., Grosse, G., Webster, J. M. and Urban, F. E.: Erosional history of Cape Halkett and contemporary monitoring of bluff retreat, Beaufort Sea coast, Alaska, *Polar Geography*, 32(3–4), 129–142, doi:10.1080/10889370903486449, 2009a.
- 20 Jones, B. M., Arp, C. D., Jorgenson, M. T., Hinkel, K. M., Schmutz, J. A. and Flint, P. L.: Increase in the rate and uniformity of coastline erosion in Arctic Alaska, *Geophys. Res. Lett.*, 36(3), L03503, doi:10.1029/2008GL036205, 2009b.
- Jones, B. M., Farquharson, L. M., Baughman, C. A., Buzard, R. M., Arp, C. D., Grosse, G., Bull, D. L., Günther, F., Nitze, I., Urban, F., Kasper, J. L., Frederick, J. M., Thomas, M., Jones, C., Mota, A., Dallimore, S., Tweedie, C., Maio, C., Mann, D. H., Richmond, B., Gibbs, A., Xiao, M., Sachs, T., Iwahana, G., Kanevskiy, M. and Romanovsky, V. E.: A decade of remotely sensed observations highlight complex processes linked to coastal permafrost bluff erosion in the Arctic, *Environmental Research Letters*, 13(11), 115001, doi:10.1088/1748-9326/aae471, 2018.
- Jorgenson, M. T. and Brown, J.: Classification of the Alaskan Beaufort Sea Coast and estimation of carbon and sediment inputs from coastal erosion, *Geo-Mar Lett*, 25(2–3), 69–80, doi:10.1007/s00367-004-0188-8, 2005.
- 30 Klemas, V. V.: Coastal and environmental remote sensing from unmanned aerial vehicles: an overview, *Journal of Coastal Research*, 1260–1267, doi:10.2112/JCOASTRES-D-15-00005.1, 2015.
- Lantuit, H. and Pollard, W. H.: Temporal stereophotogrammetric analysis of retrogressive thaw slumps on Herschel Island, Yukon Territory, *Natural Hazards and Earth System Science*, 5(3), 413–423, 2005.
- Lantuit, H. and Pollard, W. H.: Fifty years of coastal erosion and retrogressive thaw slump activity on Herschel Island, southern Beaufort Sea, Yukon Territory, Canada, *Geomorphology*, 95(1–2), 84–102, doi:10.1016/j.geomorph.2006.07.040, 2008.
- 35 Lantuit, H., Overduin, P. P., Couture, N., Wetterich, S., Aré, F., Atkinson, D., Brown, J., Cherkashov, G., Drozdov, D., Forbes, D. L., Graves-Gaylord, A., Grigoriev, M., Hubberten, H.-W., Jordan, J., Jorgenson, T., Ødegård, R. S., Ogorodov, S., Pollard,



- W. H., Rachold, V., Sedenko, S., Solomon, S., Steenhuisen, F., Streletskaia, I. and Vasiliev, A.: The Arctic Coastal Dynamics Database: A New Classification Scheme and Statistics on Arctic Permafrost Coastlines, Estuaries and Coasts, 35(2), 383–400, doi:10.1007/s12237-010-9362-6, 2012.
- 5 Mahoney, A. R., Eicken, H., Gaylord, A. G. and Gens, R.: Landfast sea ice extent in the Chukchi and Beaufort Seas: The annual cycle and decadal variability, *Cold Regions Science and Technology*, 103, 41–56, doi:10.1016/j.coldregions.2014.03.003, 2014.
- Mancini, F., Dubbini, M., Gattelli, M., Stecchi, F., Fabbri, S. and Gabbianelli, G.: Using unmanned aerial vehicles (UAV) for high-resolution reconstruction of topography: the structure from motion approach on coastal environments, *Remote Sensing*, 5(12), 6880–6898, doi:10.3390/rs5126880, 2013.
- 10 Manson, G. K., Solomon, S. M., Forbes, D. L., Atkinson, D. E. and Craymer, M.: Spatial variability of factors influencing coastal change in the Western Canadian Arctic, *Geo-Mar Lett*, 25(2–3), 138–145, doi:10.1007/s00367-004-0195-9, 2005.
- Mars, J. C. and Houseknecht, D. W.: Quantitative remote sensing study indicates doubling of coastal erosion rate in past 50 yr along a segment of the Arctic coast of Alaska, *Geology*, 35(7), 583–586, doi:10.1130/G23672A.1, 2007.
- 15 Metcalfe, D. B., Hermans, T. D. G., Ahlstrand, J., Becker, M., Berggren, M., Björk, R. G., Björkman, M. P., Blok, D., Chaudhary, N., Chisholm, C., Classen, A. T., Hasselquist, N. J., Jonsson, M., Kristensen, J. A., Kumordzi, B. B., Lee, H., Mayor, J. R., Prevéy, J., Pantazatou, K., Rousk, J., Sponseller, R. A., Sundqvist, M. K., Tang, J., Uddling, J., Wallin, G., Zhang, W., Ahlström, A., Tenenbaum, D. E. and Abdi, A. M.: Patchy field sampling biases understanding of climate change impacts across the Arctic, *Nature Ecology & Evolution*, 2(9), 1443, doi:10.1038/s41559-018-0612-5, 2018.
- 20 Myers-Smith, I. H. and Lehtonen, S.: NOAA’s Arctic: The Great Flood of July 2016, Team Shrub: Tundra Ecology Lab [online] Available from: <https://teamshrub.com/2016/07/22/noaas-arkctic-the-great-flood-of-july-2016/> (Accessed 11 February 2018), 2016.
- Myers-Smith, I. H., Grabowski, M., Thomas, H. J. D., Angers-Blondin, S., Daskalova, G., Bjorkman, A. D., Cunliffe, A. M., Assmann, J., Boyle, J., McLeod, E., McLeod, S., Joe, R., Lennie, P., Arey, D., Gordon, R. and Eckert, C.: Eighteen years of ecological monitoring reveals multiple lines of evidence for tundra vegetation change, *Ecology Monographs*, Accepted.
- 25 Obu, J., Lantuit, H., Myers-Smith, I., Heim, B., Wolter, J. and Fritz, M.: Effect of terrain characteristics on soil organic carbon and total nitrogen stocks in soils of Herschel Island, Western Canadian Arctic, *Permafrost and Periglac. Process.*, n/a-n/a, doi:10.1002/ppp.1881, 2015.
- 30 Obu, J., Lantuit, H., Fritz, M., Pollard, W. H., Sachs, T. and Guenther, F.: Relation between planimetric and volumetric measurements of permafrost coast erosion: a case study from Herschel Island, western Canadian Arctic, *Polar Res.*, 35, 30313, doi:10.3402/polar.v35.30313, 2016.
- Olynyk, D.: Buildings, in *Herschel Island - Qikiqtaryuk: A natural and cultural history of Yukon’s Arctic island*, edited by C. R. Burn, pp. 202–209, University of Calgary Press, Calgary, Canada., 2012.
- 35 Overduin, P. P., Strzelecki, M. C., Grigoriev, M. N., Couture, N., Lantuit, H., St-Hilaire-Gravel, D., Günther, F. and Wetterich, S.: Coastal changes in the Arctic, in *Sedimentary Coastal Zones from High to Low Latitudes: Similarities and Differences*, vol. 388, pp. 103–129, Geological Society, London, UK. [online] Available from: <http://sp.lyellcollection.org/content/388/1/103> (Accessed 8 February 2018), 2014.



- Ping, C.-L., Michaelson, G. J., Guo, L., Jorgenson, M. T., Kanevskiy, Shur, Y., Dou, F. and Liang, J.: Soil carbon and material fluxes across the eroding Alaska Beaufort Sea coastline, *Journal of Geophysical Research: Biogeosciences*, 116(G2), doi:10.1029/2010JG001588, 2011.
- Pollard, W.: *The Nature and Origin of Ground Ice in the Herschel Island Area, Yukon Territory.*, 1990.
- 5 Radosavljevic, B., Lantuit, H., Pollard, W., Overduin, P., Couture, N., Sachs, T., Helm, V. and Fritz, M.: Erosion and Flooding-Threats to Coastal Infrastructure in the Arctic: A Case Study from Herschel Island, Yukon Territory, Canada, *Estuaries Coasts*, 39(4), 900–915, doi:10.1007/s12237-015-0046-0, 2016.
- Rampton, V. N.: Quaternary geology of the Yukon Coastal Plain, *Bulletin, Geological Survey of Canada*. [online] Available from: <https://geoscan.nrcan.gc.ca/starweb/geoscan/servlet.starweb?path=geoscan/fulle.web&search1=R=111347>, 1982.
- 10 Retamal, L., Bonilla, S. and Vincent, W. F.: Optical gradients and phytoplankton production in the Mackenzie River and the coastal Beaufort Sea, *Polar Biol*, 31(3), 363–379, doi:10.1007/s00300-007-0365-0, 2008.
- Richter-Menge, J., Overland, J. E., Mathis, J. T. and Osborne, E.: Arctic Report Card 2017. [online] Available from: <http://www.arctic.noaa.gov/Report-Card>, 2017.
- Río, L. D. and Gracia, F. J.: Error determination in the photogrammetric assessment of shoreline changes, *Nat Hazards*, 65(3), 2385–2397, doi:10.1007/s11069-012-0407-y, 2013.
- Schuur, E. A. G., McGuire, A. D., Schädel, C., Grosse, G., Harden, J. W., Hayes, D. J., Hugelius, G., Koven, C. D., Kuhry, P., Lawrence, D. M., Natali, S. M., Olefeldt, D., Romanovsky, V. E., Schaefer, K., Turetsky, M. R., Treat, C. C. and Vonk, J. E.: Climate change and the permafrost carbon feedback, *Nature*, 520(7546), 171–179, doi:10.1038/nature14338, 2015.
- 20 Semiletov, I., Pipko, I., Gustafsson, Ö., Anderson, L. G., Sergienko, V., Pugach, S., Dudarev, O., Charkin, A., Gukov, A., Bröder, L., Andersson, A., Spivak, E. and Shakhova, N.: Acidification of East Siberian Arctic Shelf waters through addition of freshwater and terrestrial carbon, *Nature Geoscience*, 9(5), 361–365, doi:10.1038/ngeo2695, 2016.
- Serreze, M. C. and Barry, R. G.: Processes and impacts of Arctic amplification: A research synthesis, *Global and Planetary Change*, 77(1), 85–96, doi:10.1016/j.gloplacha.2011.03.004, 2011.
- 25 Solomon, S. M., Forbes, D. L. and Kierstead, B.: Coastal impacts of climate change: Beaufort Sea erosion study / S.M. Solomon, D.L. Forbes, and Brian Kierstead.: M183-2/2890E-PDF - Government of Canada Publications - Canada.ca, Geological Survey of Canada, Natural Resources Canada, Ottawa, Ontario. [online] Available from: <http://publications.gc.ca/site/eng/9.820125/publication.html> (Accessed 5 December 2018), 1993.
- Sona, G., Pinto, L., Pagliari, D., Passoni, D. and Gini, R.: Experimental analysis of different software packages for orientation and digital surface modelling from UAV images, *Earth Sci Inform*, 7(2), 97–107, doi:10.1007/s12145-013-0142-2, 2014.
- 30 Stow, D. A., Hope, A., McGuire, D., Verbyla, D., Gamon, J., Huemmrich, F., Houston, S., Racine, C., Sturm, M., Tape, K., Hinzman, L., Yoshikawa, K., Tweedie, C., Noyle, B., Silapaswan, C., Douglas, D., Griffith, B., Jia, G., Epstein, H., Walker, D., Daeschner, S., Petersen, A., Zhou, L. and Myneni, R.: Remote sensing of vegetation and land-cover change in Arctic Tundra Ecosystems, *Remote Sensing of Environment*, 89(3), 281–308, doi:10.1016/j.rse.2003.10.018, 2004.
- 35 Stroeve, J. C., Markus, T., Miller, J. and Barrett, A.: Changes in Arctic melt season and implications for sea ice loss, *Geophysical Research Letters*, 41, 1216–1225, doi:<https://doi.org/10.1002/2013GL058951>, 2014.



- Thieler, E. R., Himmelstoss, E. A., Zichichi, J. L. and Ergul, A.: The Digital Shoreline Analysis System (DSAS) Version 4.0 - An ArcGIS extension for calculating shoreline change (Ver.4.4, July 2017), USGS Numbered Series, U.S. Geological Survey, Reston. [online] Available from: <http://pubs.er.usgs.gov/publication/ofr20081278> (Accessed 23 January 2018), 2009.
- 5 Turner, I. L., Harley, M. D. and Drummond, C. D.: UAVs for coastal surveying, *Coastal Engineering*, 114, 19–24, doi:10.1016/j.coastaleng.2016.03.011, 2016.
- UNEP: Policy Implications of Warming Permafrost, UNEP. [online] Available from: <https://epic.awi.de/33086/1/permafrost.pdf>, 2012.
- UNESCO: Ivvavik / Vuntut / Herschel Island (Qikiqtaruk), UNESCO World Heritage Centre. [online] Available from: <http://whc.unesco.org/en/tentativelists/1939/> (Accessed 7 February 2018), 2004.
- 10 van Vliet, M. T. H., Franssen, W. H. P., Yearsley, J. R., Ludwig, F., Haddeland, I., Lettenmaier, D. P. and Kabat, P.: Global river discharge and water temperature under climate change, *Global Environmental Change*, 23(2), 450–464, doi:10.1016/j.gloenvcha.2012.11.002, 2013.
- Vonk, J. E., Sánchez-García, L., Dongen, B. E. van, Alling, V., Kosmach, D., Charkin, A., Semiletov, I. P., Dudarev, O. V., Shakhova, N., Roos, P., Eglinton, T. I., Andersson, A. and Gustafsson, Ö.: Activation of old carbon by erosion of coastal and subsea permafrost in Arctic Siberia, *Nature*, 489(7414), 137–140, doi:10.1038/nature11392, 2012.
- 15 Wegner, C., Bennett, K. E., Vernal, A. de, Forwick, M., Fritz, M., Heikkilä, M., Łacka, M., Lantuit, H., Laska, M., Moskalik, M., O'Regan, M., Pawłowska, J., Promińska, A., Rachold, V., Vonk, J. E. and Werner, K.: Variability in transport of terrigenous material on the shelves and the deep Arctic Ocean during the Holocene, *Polar Research*, 34(1), 24964, doi:10.3402/polar.v34.24964, 2015.
- 20 Wessel, P. and Smith, W. H. F.: Shorelines: Wessel, Pål, and Walter H. F. Smith. “A Global, Self-Consistent, Hierarchical, High-Resolution Shoreline Database.” *Journal of Geophysical Research: Solid Earth* 101, no. B4 (1996): 8741–8743. <https://doi.org/10.1029/96JB00104>, *Journal of Geophysical Research: Solid Earth*, 101(B4), 8741–8743, doi:<https://doi.org/10.1029/96JB00104>, 1996.
- 25 Westoby, M. J., Brasington, J., Glasser, N. F., Hambrey, M. J. and Reynolds, J. M.: ‘structure-from-motion’ photogrammetry: A low-cost, effective tool for geoscience applications, *Geomorphology*, 179, 300–314, doi:10.1016/j.geomorph.2012.08.021, 2012.
- Whalen, D.: Monitoring, understanding and predicting costal change in the Mackenzie-Beaufort Region, NT, Quebec City, Quebec, Canada., 2017.
- 30 Whalen, D., Fraser, R. and MacLeod, R.: The acceleration of change – how UAV technology is being used to better understand coastal permafrost landscapes in the Mackenzie-Beaufort Region, NT, ArcticNet. [online] Available from: <http://www.arcticnet.ulaval.ca/pdf/media/IRIS-1-newsletter-Dec-2017.pdf>, 2017.
- Wobus, C., Anderson, R., Overeem, I., Matell, N., Clow, G. and Urban, F.: Thermal erosion of a permafrost coastline: improving process-based models using time-lapse photography, *Arctic, Antarctic, and Alpine Research*, 43(3), 474–484, doi:10.1657/1938-4246-43.3.474, 2011.

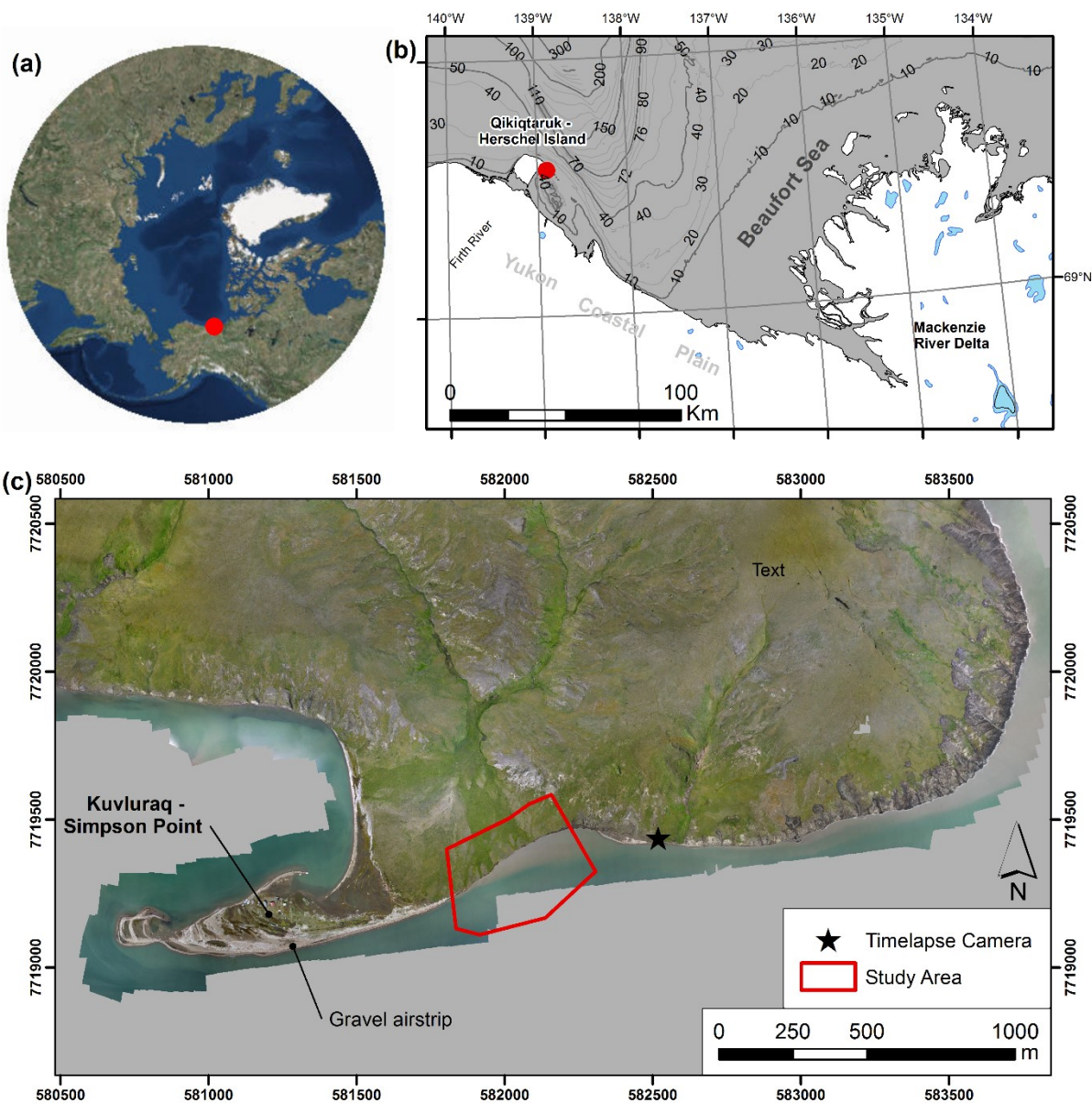


Figure 1: (a) The location of the study region in the western Canadian Arctic (Basemap from (ESRI et al., 2018), polar stereographic projection), (b) Qikiqtaruk – Herschel Island in the Beaufort Sea (shorelines from (Wessel and Smith, 1996)), and (c) true-colour orthomosaic compiled from ca. 9000 individual images collected by drone survey in August 2017 indicating the location of the 500 m study stretch and the time-lapse camera used to make the supplementary video (S1) relative to Kuvluraq – Simpson Point.

5

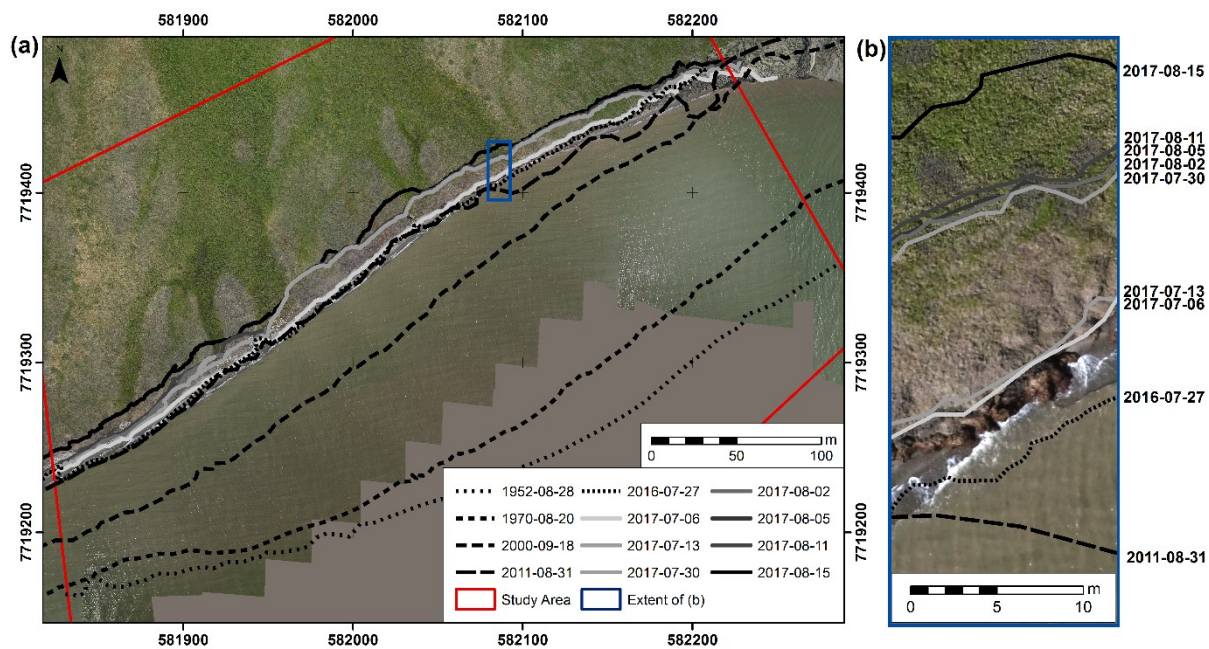


Figure 2. (a) Overview of the 500 m study area, illustrating all twelve shoreline positions since 1952 overlaid on the 2017-07-06 orthomosaic. (b) Ten-fold magnification in scale, illustrating the episodic nature of the shoreline changes at this location.

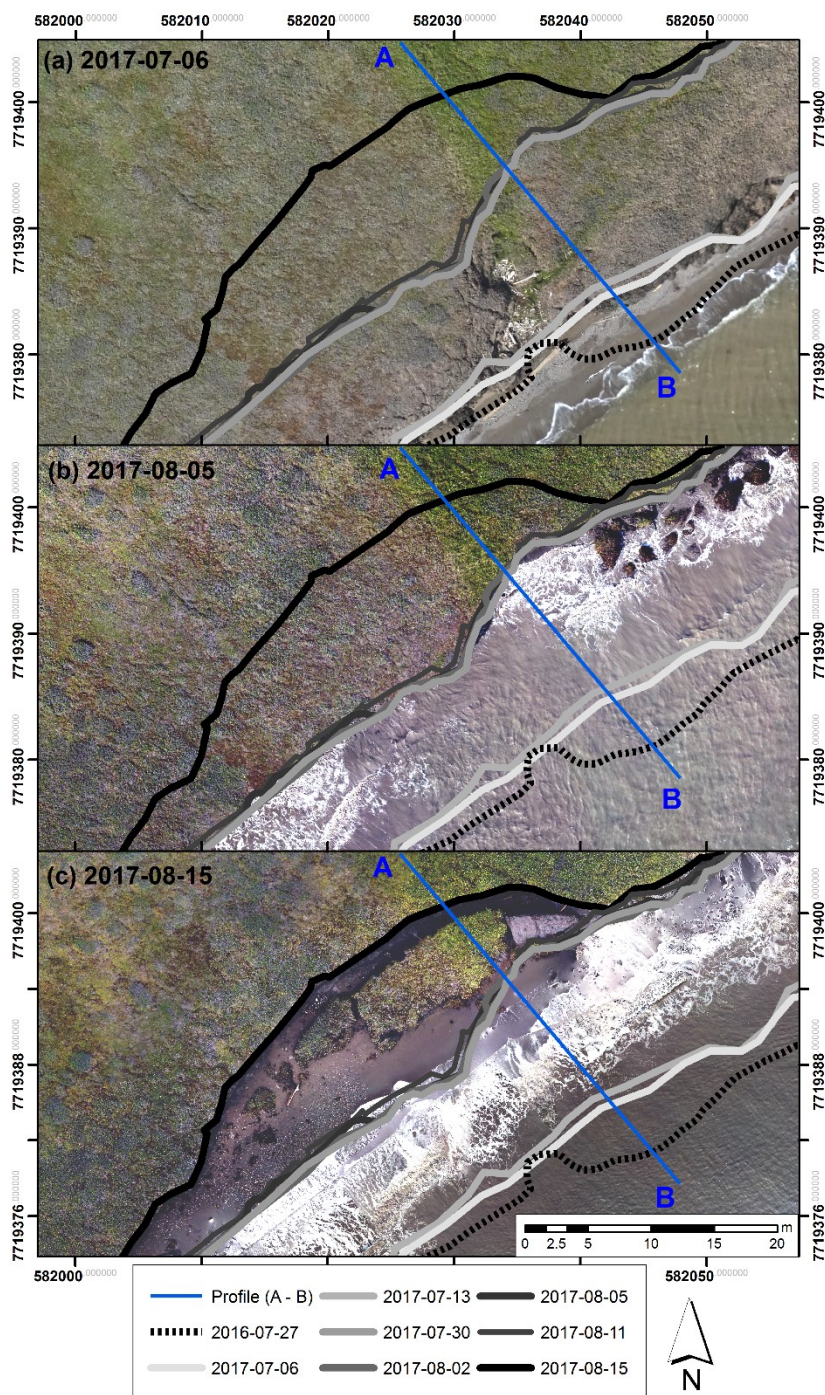
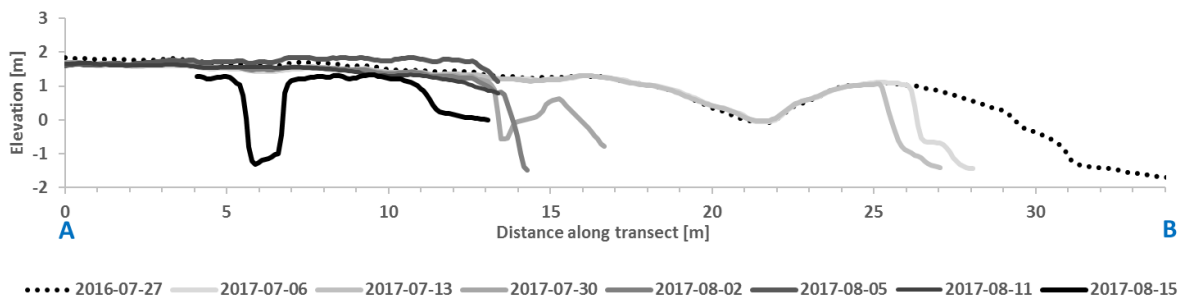


Figure 3. Shoreline positions between 2016 and 2017 overlaid on three orthomosaics for part of the study reach. The blocks shown in (c) were detached from the bluff, with water moving freely behind during periods of higher water level (see figure S3). Profile A-B indicates the horizontal position of the cross-sectional profiles discussed in section 4.2 and depicted in Figure 4.



5 **Figure 4.** Elevation profiles along the A-B transect shown in Figure 3, extracted from digital surface models obtained by the structure-from-motion modelling of the drone-acquired images (no vertical exaggeration). Note that two of the latter elevation models (from 2017-08-05 and 2017-08-15) both suffered from datum problems due to insufficient spatial constraint; see discussion for details.

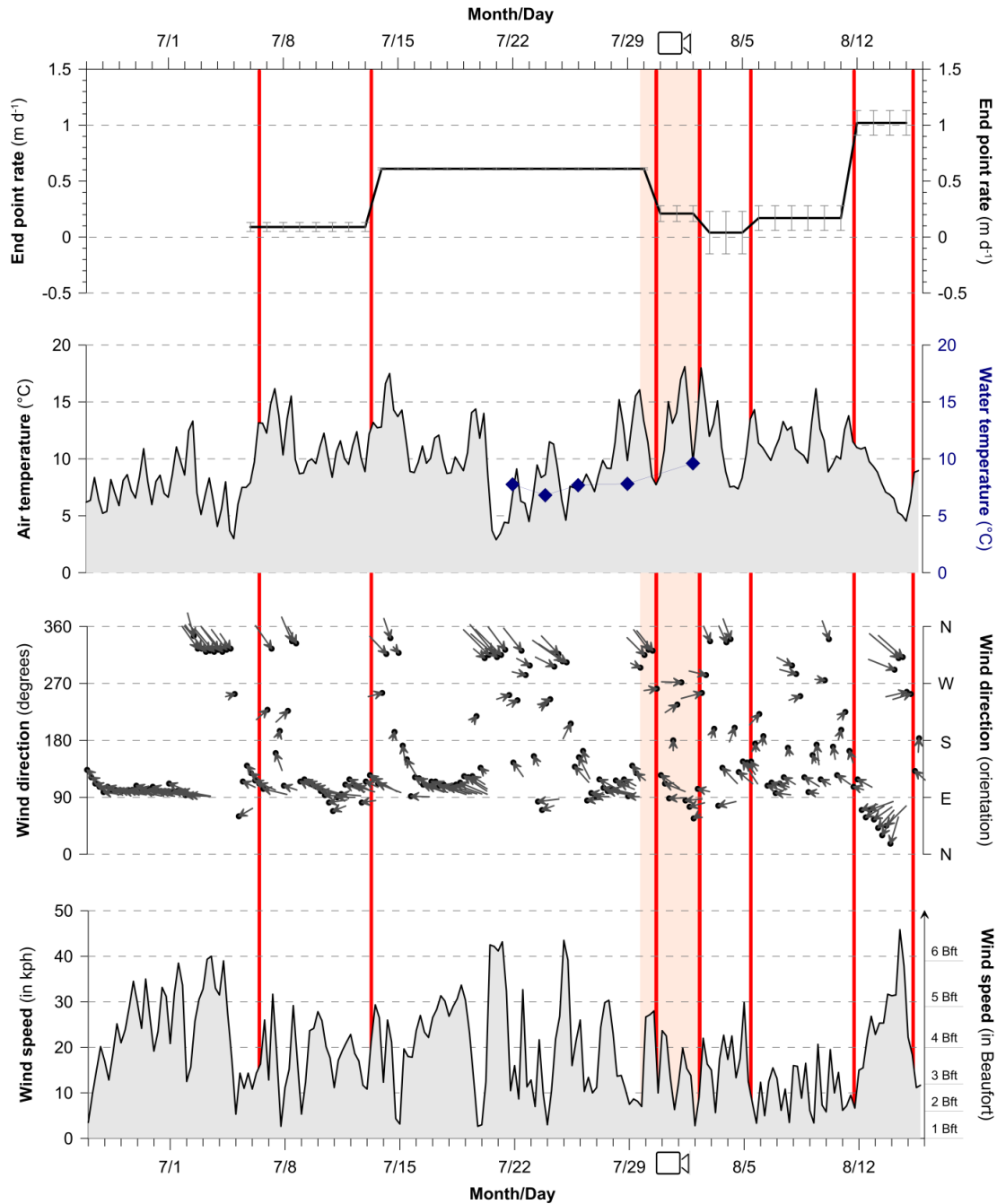


Figure 5. Shoreline retreat (end point) rates normalised by day for each observation period in 2017, six-hour moving averages of air temperature, wind direction, and wind velocity in July-August 2017 (data from Environment Canada, 2017). Dates and times of aerial surveys are indicated by the red bars, point measurements of sea surface temperature from CTD casts are indicated by blue diamonds (see Figure S3 for full CTD profiles), and the duration of time-lapse survey shown in video S1 is indicated by the red shading.



Table 1. Dataset and shoreline position parameters. The approximate times of drone surveys are in local time (UTC -08:00). Shoreline uncertainties are a combination of (i) image co-registration (root mean square (RMS) error of ground control points (GCPs)), (ii) image quality (pixel error), and (iii) shoreline mapping (digitizing) error.

Observation date	Image Type	Images [n]	Scale	GCPs [n]	Georeferencing		RMS	Pixel Error [m]	Digitisi ng Error [m]	Total Shoreline Uncertainty [m]
					Georeferencing Error [m]					
					Absolute	Relative				
					(NAD83)					
1952-08-28	Panchromatic aerial photograph	1	1:70000	11	-	2.475	3.50	4.00	9.975	
1970-08-20	Panchromatic aerial photograph	1	1:12000	19	-	1.117	0.60	2.00	3.717	
2000-09-18	Panchromatic Ikonos photograph	1	-	19	-	5.087	1.00	2.00	8.137	
2011-08-31	Panchromatic GeoEye photograph	1	-	17	-	0.330	0.50	1.50	2.330	
2016-07-27	RGB orthomosaic (Drone – FX-61)	1	-	26	0.015	-	0.03	0.15	0.195	
2017-07-06 @ 12:20	RGB orthomosaic (Drone – FX-61)	1325	-	98	0.063	Base Image	0.02	0.10	0.183	
2017-07-13 @ 08:30	RGB orthomosaic (Drone – FX-61)	194	-	13	0.043	-	0.02	0.10	0.163	
2017-07-30 @ 18:00	RGB orthomosaic (Drone - Phantom)	383	-	5	0.037	-	0.02	0.10	0.157	
2017-08-02 @ 08:00	RGB orthomosaic (Drone - Phantom)	2040	-	22	0.021	-	0.02	0.10	0.141	
2017-08-05 @ 11:40	RGB orthomosaic (Drone - Phantom)	336	-	6	0.443	-	0.02	0.10	0.563	
2017-08-11 @ 17:00	RGB orthomosaic (Drone – FX-61)	8994	-	132	0.167	-	0.04	0.10	0.307	
2017-08-15 @ 10:20	RGB orthomosaic (Drone - Phantom)	402	-	3	0.178	-	0.02	0.10	0.298	



5 Table 2. Summary of shoreline change for all periods, in terms of net shoreline change and end-point rates. Net shoreline change is the distance between the oldest and youngest shorelines. End-point rate is the net shoreline change normalised by time (years or days, for supra- or sub-annual periods, respectively), where SD is standard deviation and DOA is Dilution of Accuracy (from Equation 1).

Period	Days	Mean Shoreline Change ± SD (m)	Net Mean End Point Rate ± DOA (m·a⁻¹)	(m·d⁻¹)
<u>Supra-annual periods</u>				
1952-08-28 – 1970-08-20	6 567	20.7 ± 10.6	1.2 ± 0.6	
1970-08-20 – 2000-09-18	10 986	69.2 ± 21.9	2.3 ± 0.3	
2000-09-18 – 2011-08-31	3 986	33.0 ± 11.1	3.0 ± 0.8	
2011-08-31 – 2016-07-27	1 791	3.5 ± 4.6	0.7 ± 0.5	
2016-07-27 – 2017-07-06	344	2.9 ± 2.2	3.1 ± 0.3	
1952-08-28 – 2017-08-15	23 735	143.7 ± 28.4	2.2 ± 0.2	<0.01 ± 0.00
<u>Sub-annual periods</u>				
2017-07-06 – 2017-07-13	7	0.5 ± 0.5		0.09 ± 0.04
2017-07-13 – 2017-07-30	17	7.4 ± 5.6		0.61 ± 0.01
2017-07-30 – 2017-08-02	3	0.6 ± 1.1		0.21 ± 0.07
2017-08-02 – 2017-08-05	3	0.1 ± 0.4		0.04 ± 0.19
2017-08-05 – 2017-08-11	6	1.0 ± 0.4		0.17 ± 0.11
2017-08-11 – 2017-08-15	4	4.1 ± 1.1		1.02 ± 0.11
2017-07-06 – 2017-08-15	40	14.5 ± 3.2		0.36 ± 0.01